Butyrophenone on O-TiO_2(110): One-Dimensional Motion in a Weakly Confined Potential Well

Stephen C. Jensen,[†] Alex Shank,[†] Robert J. Madix,[‡] and Cynthia M. Friend[†,*]

[†]Department of Chemistry and Chemical Biology and [‡]School of Engineering and Applied Sciences, Harvard University, Cambridge, Massachusetts 02138, United States

ABSTRACT

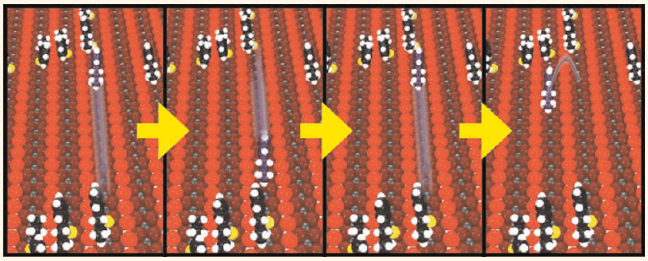

We demonstrate the one-dimensional confinement of weakly bound butyrophenone molecules between strongly bound complexes formed *via* reaction with oxygen on TiO_2(110). Butyrophenone weakly bound to Ti rows through the carbonyl oxygen diffuses freely in one dimension along the rows even at 55 K, persisting for many minutes before hopping out of the 1-D well. Quantitative analysis yields an estimate of the migration barrier of 0.11 eV and a frequency factor of 6.5×10^9 Hz. These studies demonstrate that weakly bound organic molecules can be confined on a surface by creating molecular barriers, potentially altering their assembly.

KEYWORDS: titanium dioxide · STM · DFT · confined · 1-D gas · ketones

Surface diffusion is generally important in interfacial processes, such as self-assembly[1] or heterogeneous catalysis.[2] Maximizing the desired electron transport, stability, or reactivity in these applications often requires optimization of the interactions between adjacent molecules through orientation, transport, and confinement. Due to the complexity of many of these systems, reducing dimensionality can often aid in this optimization.

Diffusion has been extensively studied on metal surfaces:[3,4] for example, anisotropic transport of CO_2 utilizing dithioanthracene as a carrier on Cu(111),[5] hydrogen-assisted mobilization of platinum atoms on Pt(110),[6] and nanoscale confinement of CO using an anthraquinone network on Cu(110).[7] There have been fewer studies on metal oxides, though anisotropic diffusion of strongly bound organics has been reported on rutile TiO_2(110) surfaces.[8]

Herein we use butyrophenone as a model for studying surface-bound gases due to its conjugated phenyl ring—a key functional group in many polymers used to facilitate electron transfer (Figure 1A).[9] Ketones, including butyrophenone, weakly bind to the five-fold coordinated Ti atoms (Ti_{5c}) along the rows of the rutile TiO_2(110) surface (Figure 1B) through the carbonyl oxygen in the molecule,[10−12] as indicated by our density functional theory (DFT) studies of butyrophenone described below (Figure 1C). The diffusion barrier for ketones along the Ti rows is lower than for hopping perpendicular to the rows because of the loss of this coordination when traversing the intervening oxygen.

Butyrophenone also reacts with oxygen atoms adsorbed on the Ti_{5c} atoms (Figure 1B), creating a strongly bound complex on the Ti_{5c} row (Figure 1D).[10,11] Since these complexes can be widely spaced along the row, they afford an ideal system for investigating one-dimensional diffusion along the rows.

RESULTS AND DISCUSSION

Formation of anchored butyrophenone−O complexes from reaction with O adatoms on TiO_2(110) is directly observable by STM (Figures 2A,B and Figure 4). In the example shown, the coverage of O adatoms on the surface is 0.08 monolayers (ML). The coverage of anchored complexes is 0.07 ML, clearly suggesting the reaction of a single butyrophenone with a single adsorbed oxygen atom to form the complex (1 ML = 1 molecule per Ti_{5c} = 5.2×10^{14} cm^{-2}). They are generally separated by up to 9 unit cells. The oval-shaped features suggest that the phenyl ring and the alkyl chain are oriented along the Ti rows. The width of the complex is $0.83 \times 0.57 \pm 0.06$ nm, consistent with the size of

* Address correspondence to cfriend@seas.harvard.edu.

Received for review October 6, 2011 and accepted March 27, 2012.

Published online March 27, 2012
10.1021/nn300949q

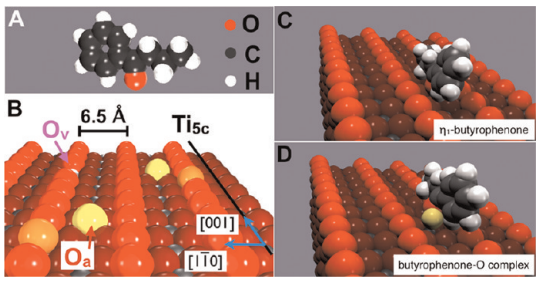

Figure 1. Molecular models of (A) butyrophenone; (B) TiO_2-(110) surface containing oxygen adatoms (yellow) and filled bridging oxygen vacancies (light orange); (C) butyrophenone—the lowest structure sampled disposes the carbonyl O over Ti_{5c} atom (binding energy = 0.87 eV); (D) for the butyrophenone−O complex (binding energy = 1.05 eV). The butyrophenone−O complex shown is the lowest energy state studied using DFT; however, an exhaustive search of all structures was not possible.

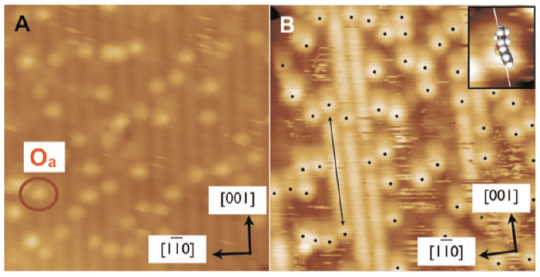

Figure 2. Scanning tunneling microscope (STM) images demonstrrate the formation of a 1-D gas of butyrophenone confined between strongly bound oxygen complexes. STM images of (A) the TiO_2(110) surface containing oxygen adatoms (O_a) after exposure of a freshly prepared surface to O_2 and (B) the strongly bound butyrophenone−oxygen complex (inset and marked by black dots) and butyrophenone adsorbed one-dimensionally along the Ti cation rows (bright lines) after exposure of (A) to 0.25 monolayers of butyrophenone at 55 K, warming to 300 K for 5 min, followed by cooling and imaging at 55 K. The inset indicates a superimposed model of the strongly bound complex. The scan rate is 300 nm/s, and image sizes are 10.4 × 10.4 nm^2; the inset in (B) is 1.00 × 1.25 nm^2.

butyrophenone estimated from van der Waals radii (Figure 2B inset). The orientation of the phenyl and alkyl chain appears to be different from that of acetone−O complexes, in which the methyl groups apparently orient perpendicular to Ti rows.[10,12,15] This difference may be due to repulsive interactions of the large R groups with the bridging oxygen rows.

The formation of the strongly bound butyrophenone−oxygen complex at 300 K was observed in STM images taken sequentially (Figure 3). The O adatoms were formed initially by treatment of the TiO_2(110) surface with a saturation coverage (300 L) of O_2 followed by heating to above 120 K.[13,14] Butyrophenone was admitted to the vacuum chamber for 2 min at room temperature at 1×10^{-10} mbar while scanning. Small circular features along the Ti rows in Figure 3A are attributable to oxygen adatoms, and they are present prior to dosing butyrophenone; the larger features are butyrophenone−oxygen complexes that have already formed. During this exposure, an oxygen adatom can be seen converting to a bright feature characteristic of the butyrophenone−O complex (Figure 3B). This feature is then immobile, consistent with the stronger binding energy of the butyrophenone complex compared to the free ketone (Figure 3C,D). These features are *only* observed if oxygen adatoms are present on the surface during butyrophenone deposition, and they are stable for several days at 300 K in the STM.

The immobile complexes restrict the diffusion of the coadsorbed butyrophenone weakly bound within the Ti_{5c} channels (Figure 4). During imaging at 55 K, diffuse bands composed of horizontal streaks along the scan direction, which we attribute to mobile butyrophenone, appear along the Ti_{5c} rows between two butyrophenone complexes. These features vary from frame-to-frame, as is characteristic of a mobile gas randomly diffusing along the Ti_{5c} rows.[16,17] The mobile butyrophenone molecule occasionally escapes from the channel, based on the disappearance of streaks along a given row. Typical residence times within the rows are greater than 30 min at 55 K (Figure 4C,D). The streaks disappear after heating to the desorption temperature of butyrophenone but lower than the temperature for decomposition of the complex, confirming that they are due to molecularly adsorbed butyrophenone. The 1-D gas likely persists because the butyrophenone−O complexes exert van der Waals repulsive forces on the mobile species, and the asymmetry in the surface structure leads to confinement of the mobile species along a line.

After a period of time, the molecule can diffuse out of the potential well. We employ nudged elastic band methods and find a barrier of +0.79 eV for butyrophenone to diffuse over an oxygen row (see Supporting Information). The calculated value for the barrier represents an upper bound due to the lack of inclusion of van der Waals forces and because the molecule will likely reorient to find the lowest barrier.

The motion of the butyrophenone along a line between two butyrophenone−O complexes is clearly observed in STM movies at 55 K (movie S1 in Supporting Information). A 1-D confined random walk (movie S2) schematically illustrates the expected diffusion rates over 1 s. The tunneling parameters used in our experiments were selected to minimize tip effects[8,14,15] (+1.9 V, 40 pA), and 1-D motion was observed for a variety of tip conditions (+2.0−2.4 V and up to 0.1 nA) and scan orientations, all suggesting that tip effects are not responsible for the motion observed in our experiments.

One-dimensional intensity traces along different rows illustrate the random walk of the trapped, mobile butyrophenone (Figure 4E). The molecular position is captured in the short scan time across the row, but in the next scan across the row, the molecule may have moved. In contrast, the butyrophenone−O complexes

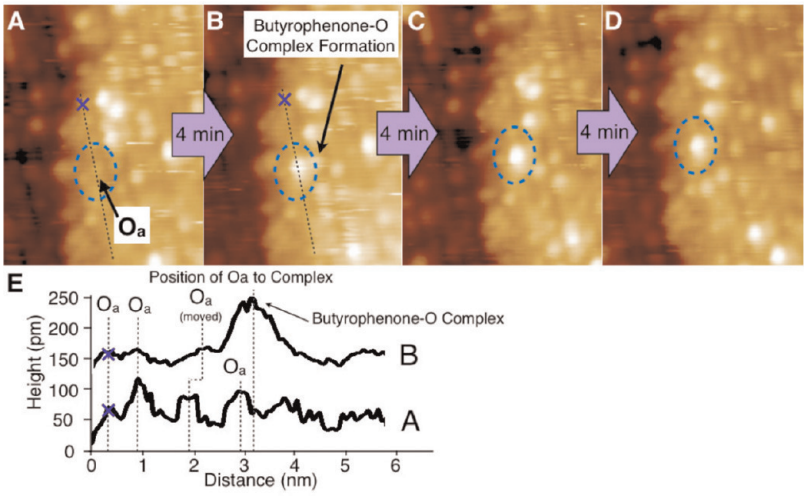

Figure 3. (A) Oxidized TiO_2(110) surface with characteristic oxygen adatoms on the Ti rows. (Circled, B) Butyrophenone−oxygen complex appears after dosing butyrophenone, (C,D) newly formed butyrophenone−oxygen complex is immobilized after reaction (T = 300 K, V = +1.6 V, i = 0.14 nA, scan rate = 300 nm/s, 6.7 × 8.9 nm^2 for all images). (E) Line scan of dotted traces in A and B showing that the oxygen adatom indicated in A reacts with butyrophenone to form an oxygen complex in spatial agreement with Figure 1D.

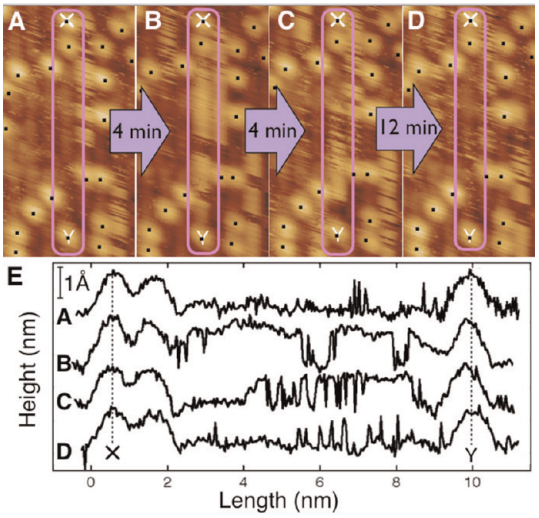

Figure 4. Molecular motion of the 1-D gas of butyrophenone traveling along a Ti_{5c} row, confined by two butyrophenone−O complexes (circled) is imaged using STM: (A) anchored complexes with diffusing butyrophenone. One row is shown before a mobile butyrophenone molecule enters the bounded row (4.9 × 9.2 nm^2). (B) Four minutes later, butyrophenone migrates along this Ti_{5c} row after entering the well. (C) Diffusing molecule remains bound in the weak potential well (same size), though its excursion appears reduced. (D) Mobile butyrophenone species diffuses out of the bounded Ti row and is no longer imaged within the Ti row (same size) (T = 55 K, V = +1.9 V, i = 40 pA, scan rate 300 nm/s). (E) Corresponding line traces along the confined 1-D potential wells in scans A−D (X and Y denote the beginning and end of the line scan, respectively). The scan rate is 150 nm/s, and it takes approximately 1 ms to traverse across a Ti row. Bright features with black dots mark the position of every butyrophenone−O complex in the images.

are immobile. Thus, tunneling current indicates the presence of a molecule at a particular point on the row at the time the row is scanned. Here, mobile butyrophenone images display consistent heights along the row while butyrophenone−oxygen complexes have a taller apparent height (0.13 nm) and lie on the ends of each confined 1-D gas. Traces A and D illustrate a row that has little confined gas motion, while traces B and C demonstrate that one or more mobile butyrophenone molecules diffuse nearly along the entire length of the channel during the scan.

The 1-D diffusion rate of mobile butyrophenone trapped in a row was probed by measuring current *versus* time using STM[18] by hovering the tip over a specific point with the feedback turned off. Measurements made between two static complexes clearly show the hopping of a weakly bound butyrophenone along the row at a rate of one hop every few milliseconds (Figure 5). The variation in tunneling current over time results from mobile butyrophenone passing under or away from the tip−tunnel junction.

The bright, nearly circular features in the STM images in Figure 4 are due to the butyrophenone−O complexes; they have a characteristic dimension of 0.57 nm. The apparent characteristic size of the hopping butyrophenone is 0.47 nm, as indicated by the length of the streaks it creates when imaged. Thus, the "on/off" event comprises movement of the adsorbed butyrophenone by between 1 and 2 nearest Ti−Ti sites. Thus, the characteristic hopping length measured by the stationary tip is 1−2 times the actual single hop Ti−Ti distance. The ratio between the hopping time for a single hop (X_1, t_1) and a hop to the next-nearest-neighbor binding site (X_2, t_2) is 4, according to the random walk analysis. Thus, even if t_2 is measured, it will affect the measured pre-exponential factor for hopping only by a small factor.

The effect of temperature on the butyrophenone diffusion rate was measured in order to quantify the parameters governing the hopping rate. The data were fit to an

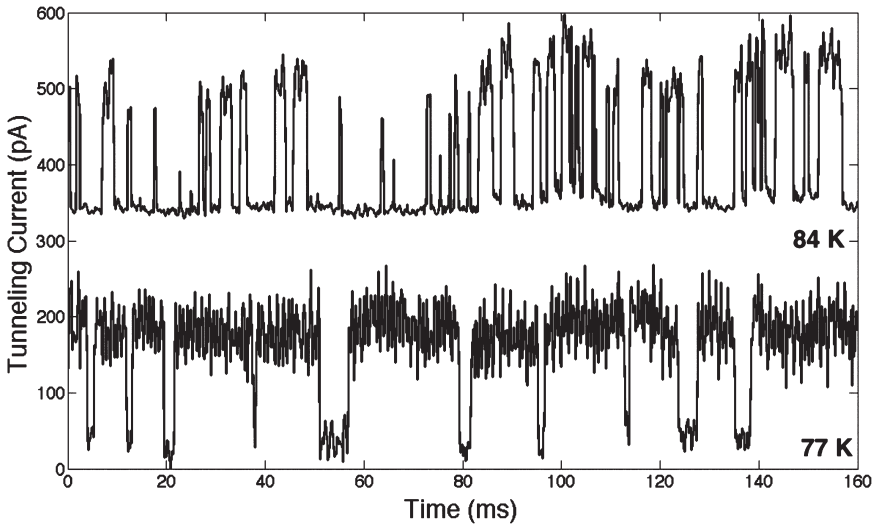

Figure 5. Diffuse motion of the 1-D butyrophenone is observed using single-molecule conductivity plots at 77 and 84 K. The STM tip feedback is turned off, and measurements were taken at +2.3 V and 300 pA hovering over a particular location. Mobile butyrophenone trace has a stepped appearance from a molecule diffusing under the hovering tip.

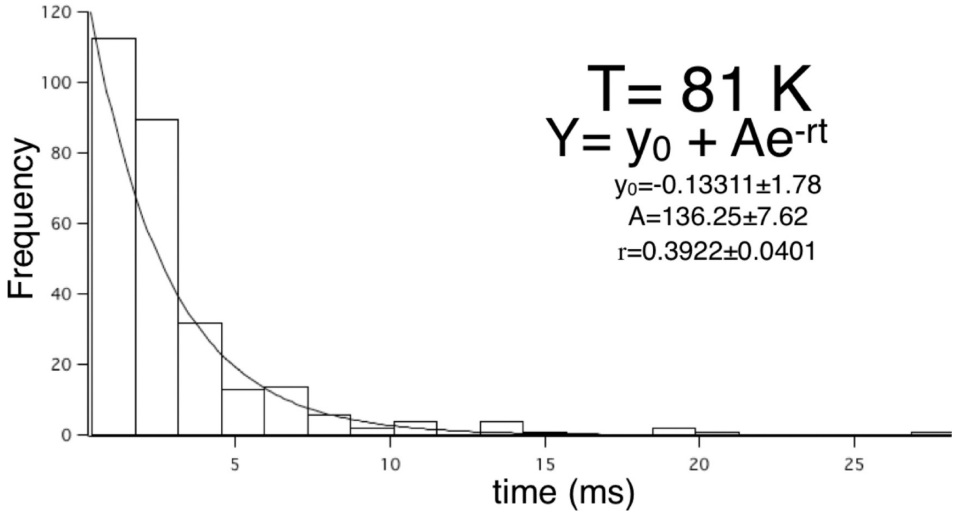

Figure 6. Distribution of dwell times for molecular butyrophenone at a specific site at 81 K within the 1-D channels on TiO_2. Traces were sampled every 160 μs for 150 ms, and dwell times were calculated from widths of the "spikes" in Figure 5 ($V = +2.3$ V, $i = 30$ pA).

Arrhenius plot, $r = A\exp[-E_d/k_BT]$, where r is the hopping rate, A is the attempt frequency, E_d is the diffusion barrier, T is temperature, and k_B is Boltzmann's constant. The hopping rate was calculated by measuring the residence time in a current−time trace of mobile butyrophenone for hundreds of events at four different temperatures (74, 77, 81, and 84 K) and creating a histogram of residence times for each temperature. A single exponential, $Y = y_0 + A\exp(-rt)$, was fit to the data, with r the hopping rate for that temperature (Figure 6). A plot of ln(r) *versus* $1/T$ gives a migration barrier of 0.11 ± 0.01 eV and a pre-exponential of 6(±5) × 10^9 Hz (Figure 7). The hopping rate estimated from these parameters is approximately one per second at 55 K, consistent with the streaks and diffuse bands observed. We did not observe a statistical difference in residence time based on well length.

Though the butyrophenone−O complexes were significantly less mobile than the butyrophenone itself, movement of a complex both along the Ti row and across to neighboring Ti rows was occasionally observed (Figure S1). However, the dissociation of the complex, leaving an oxygen adatom, was **not** observed at 55 K. The difference in the mobility of the butyrophenone and butyrophenone−O complex is consistent with the strength of their binding to the surface estimated from with density functional theory (Supporting Information, Figures S2−S4). The ratio of the diffusion to the desorption energy of mobile butyrophenone allows us to estimate the diffusion barrier of the complex given the calculated desorption energy and results in a 10^4 difference in mobility between the two species at 55 K.[19,20]

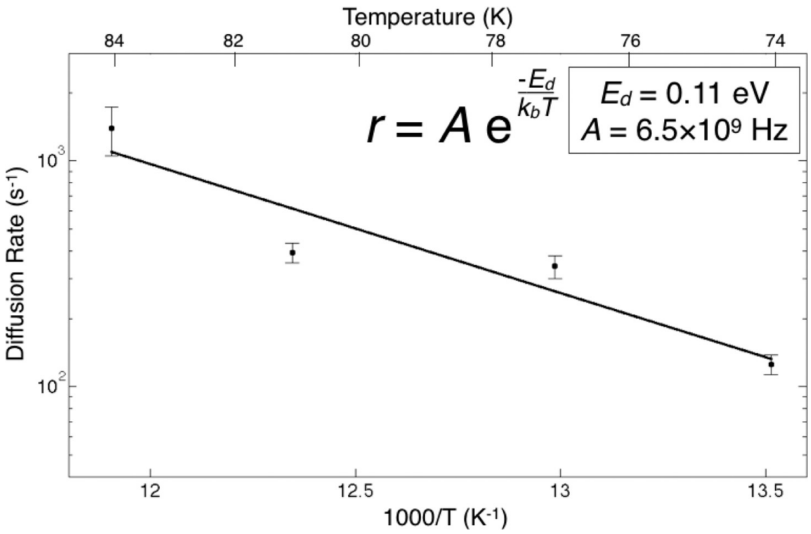

Figure 7. Arrhenius plot of mobile butyrophenone hopping rates on oxidized TiO_2(110) at different temperatures calculated from hundreds of $I(t)$ traces similar to Figure 4. Circles represent measured hopping rates at different temperatures. Assuming a thermally activated hopping rate, the activation barrier and attempt frequency can be calculated by fitting results to $\ln(r) = \ln(A) - E_d/K_B \times T^{-1}$.

CONCLUSIONS

Mobile butyrophenone can be weakly confined in a 1-D potential well on TiO_2(110) along five-fold coordinated titanium rows by using strongly bound butyrophenone−oxygen complexes. STM movies at 300 K confirm that the complexes are formed by a reaction of butyrophenone with oxygen adatoms. The mobile butyrophenone diffuses in the weakly confining 1-D potential wells with a residence time of many minutes at 55 K with a hopping rate of one per second.

EXPERIMENTAL METHODS

Software. We used Scanning Probe Image Processor v4.5.8 by Image Metrology for all image processing. All images were calibrated in the X and Y to the unit cell of TiO_2(110), which measure 0.65 nm by 0.296 nm, respectively. The Z was calibrated off the step edge which measures 0.32 nm for TiO_2(110). Density functional theory calculations described here were made using a plane wave code implemented with the Vienna Ab Initio Simulation Package (VASP). We used PAW pseudopotentials and the GGA-PW91 functional that are commonly used with TiO_2(110). We used a (5 × 2) unit cell with 4-trilayer thickness and a vacuum layer of 10 Å above. The upper two trilayers were relaxed, while the bottom two layers were fixed at their optimized bulk distances. The dipole correction has been used to minimize interactions between repeating images. A plane wave cutoff of 400 eV was used with Gaussian smearing of 0.2 eV and the 2 × 3 × 1 special Monkhorst-Pack k-point mesh. Convergence was tested by varying the cutoff up to 700 eV, the Gaussian smearing from 0.05 to 0.5 eV, and independently varying the k-point mesh in the x and y from (2 × 2 × 1) to (5 × 5 × 1), and varying the vacuum layer from 10 to 20 Å. In all cases, the convergence was below 0.05 eV. The (6 × 2) and the (7 × 2) unit cells were also compared against the (5 × 2) unit cell for the binding of butyrophenone in the parallel configuration, and the energies differed by less than 0.02 eV. Climbing nudged elastic band (cNEB) calculations were conducted by creating three images between two fixed, previously relaxed geometries at a reduced force threshold of 0.02 eV/Å.

STM. Single-crystal rutile TiO_2(110) crystals were purchased from SurfaceNet and prepared in ultrahigh vacuum by cycles of Ar^+ bombarding at 1 kV for 20 min and annealing to 1000 K for 3−5 min with a doped silicon wafer that is sandwiched below the crystal and calibrated previously using a type K thermocouple. Usually, 20−30 cycles are required before obtaining an atomically clean surface free of contaminants or calcium. The surface used in our studies initially has 3.2 × 10^{13} bridging oxygen vacancies/cm^2 on the surface (~6%), similar to what is reported in the literature. Resistivity measurements for the crystal are ~86 Ω·cm. O adatoms form *via* reaction of gaseous O_2 with various defects, including bridging oxygen vacancies and reduced interstitial Ti species, healing vacancies, and leaving the adatoms on the surface (Figure 2A).[13,14] Although the mechanism for O adatom formation is still disputed, there is general agreement about their formation and their subsequent interaction with, for example, acetone.[10−12,15] Current−time traces measured the current every 160 μs for 160 ms.

Conflict of Interest: The authors declare no competing financial interest.

Acknowledgment. We acknowledge support by the Chemistry Division of the National Science Foundation (NSF) under award No. CHE-0545335. S.J. acknowledges support by NSF for a GRFP. A.S. was supported by the Department of Defense NDSEG Program. R.J.M. acknowledges support. We thank Bingjun Xu and Derek Butcher for helpful discussions.

Supporting Information Available: Supporting Figures S1−S4, corresponding text, and supporting movies S1 and S2. This material is available free of charge *via* the Internet at http://pubs.acs.org.

REFERENCES AND NOTES

1. Tao, C.; Liu, Q.; Riddick, B.; Cullen, W.; Reutt-Robey, J.; Weeks, J.; Williams, E. Dynamic Interfaces in an Organic Thin Film. *Proc. Natl. Acad. Sci. U.S.A.* **2008**, *105*, 16418–16425.
2. Ertl, G. Oscillatory Kinetics and Spatio-Temporal Self-Organization in Reactions at Solid Surfaces. *Science* **1991**, *254*, 1750–1755.
3. Stranick, S. J.; Kamna, M. M.; Weiss, P. S. Atomic-Scale Dynamics of a Two-Dimensional Gas−Solid Interface. *Science* **1994**, *266*, 99–102.

4. Barth, J. V.; Zambelli, T.; Wintterlin, J.; Schuster, R.; Ertl, G. Direct Observation of Mobility and Interactions of Oxygen Molecules Chemisorbed on the Ag(110) Surface. *Phys. Rev. B* **1997**, *55*, 12902–12905.
5. Wong, K.; Pawin, G.; Kwon, K.; Lin, X.; Jiao, T.; Solanki, U.; Fawcett, R.; Bartels, L.; Stolbov, S.; Rahman, T. A Molecule Carrier. *Science* **2007**, *315*, 1391–1393.
6. Horch, S.; Lorensen, H.; Helveg, S.; Lægsgaard, E.; Stensgaard, I.; Jacobsen, K.; Norskov, J.; Besenbacher, F. Enhancement of Surface Self-Diffusion of Platinum Atoms by Adsorbed Hydrogen. *Nature* **1999**, *398*, 134–136.
7. Cheng, Z.; Wyrick, J.; Luo, M.; Sun, D.; Kim, D.; Zhu, Y.; Lu, W.; Kim, K.; Einstein, T.; Bartels, L. Adsorbates in a Box: Titration of Substrate Electronic States. *Phys. Rev. Lett.* **2010**, *105*, 066104.
8. Li, S.; Chu, L.; Gong, X.; Diebold, U. Hydrogen Bonding Controls the Dynamics of Catechol Adsorbed on a TiO_2-(110). *Surf. Sci.* **2010**, *328*, 882–884.
9. Goh, C.; Coakley, K. M.; McGehee, M. D. Nanostructuring Titania by Embossing with Polymer Molds Made from Anodic Alumina Templates. *Nano Lett.* **2005**, *5*, 1545–1549.
10. Henderson, M. Acetone Chemistry on Oxidized and Reduced TiO_2(110). *J. Phys. Chem. B* **2004**, *108*, 18932–18941.
11. Henderson, M. Photooxidation of Acetone on TiO_2(110): Conversion to Acetate *via* Methyl Radical Ejection. *J. Phys. Chem. B* **2005**, *109*, 12062–12070.
12. Márquez, A.; Plata, J.; Sanz, J. Role of Coverage and Surface Oxidation Degree in the Adsorption of Acetone on TiO_2-(110). A Density Functional Study. *J. Phys. Chem. C* **2009**, *113*, 19973–19980.
13. Epling, W.; Peden, C.; Henderson, M.; Diebold, U. Evidence for Oxygen Adatoms on TiO_2 (110) Resulting from O_2 Dissociation at Vacancy Sites. *Surf. Sci.* **1998**, *412*, 333–343.
14. Du, Y.; Deskins, N.; Zhang, Z.; Dohnalek, Z.; Dupuis, M.; Lyubinetsky, I. Formation of O Adatom Pairs and Charge Transfer Upon O_2 Dissociation on Reduced TiO_2(110). *Phys. Chem. Chem. Phys.* **2010**, *12*, 6337–6344.
15. Yasuo, M.; Sasahara, A.; Onishi, H. Acetone Adsorption on Oxidized and Reduced TiO_2(110): A Scanning Tunneling Microscope Study. *J. Phys. Chem. C* **2010**, *114*, 14579–14582.
16. Berner, S.; Brunner, M.; Ramoino, L.; Suzuki, H.; Guntherodt, H.; Jung, T. Time Evolution Analysis of a 2D Solid−Gas Equilibrium: A Model System for Molecular Adsorption and Diffusion. *Chem. Phys. Lett.* **2001**, *348*, 175–181.
17. Jensen, S.; Baber, A.; Tierney, H. Dimethyl Sulfide on Cu{111}: Molecular Self-Assembly and Submolecular Resolution Imaging. *ACS Nano* **2007**, *1*, 423–426.
18. Tierney, H. L.; Baber, A. E.; Sykes, E. C. H.; Akimov, A.; Kolomeisky, A. B. Dynamics of Thioether Molecular Rotors: Effects of Surface Interactions and Chain Flexibility. *J. Phys. Chem. C* **2009**, *113*, 10913–10920.
19. Baber, A. E.; Jensen, S. C.; Sykes, E. C. H. Dipole-Driven Ferroelectric Assembly of Styrene on Au{111}. *J. Am. Chem. Soc.* **2007**, *129*, 6368–6369.
20. Seebauer, E.; Allen, C. Estimating Surface Diffusion Coefficients. *Prog. Surf. Sci.* **1995**, *49*, 265–330.